

Transparent and Clinically Interpretable AI for Lung Cancer Detection in Chest X-Rays

Amy Rafferty¹[0000-0002-5120-966X], Rishi Ramaesh², and Ajitha Rajan¹

¹ University of Edinburgh, 10 Crichton St, Edinburgh EH8 9AB

² NHS Lothian, Edinburgh

Abstract. The rapidly advancing field of Explainable Artificial Intelligence (XAI) aims to tackle the issue of trust regarding the use of complex black-box deep learning models in real-world applications. Existing post-hoc XAI techniques have recently been shown to have poor performance on medical data, producing unreliable explanations which are infeasible for clinical use. To address this, we propose an ante-hoc approach based on concept bottleneck models that introduces for the first time clinical concepts into the classification pipeline, allowing the user valuable insight into the decision-making process. On a large public dataset of chest X-rays and associated medical reports, we focus on the binary classification task of lung cancer detection. Our approach yields improved classification performance on lung cancer detection when compared to baseline deep learning models ($F1 > 0.9$), while also generating clinically relevant and more reliable explanations than existing techniques. We evaluate our approach against post-hoc image XAI techniques LIME and SHAP, as well as CXR-LLaVA, a recent textual XAI tool that operates in the context of question answering on chest X-rays.

Keywords: Explainable AI (XAI) · Interpretability · Medical Imaging · Ante-hoc explanations · Post-hoc explanations · AI-Assisted diagnostics.

1 Introduction

Artificial Intelligence (AI) has recently seen extensive application in the field of medical diagnostics, revolutionizing the sector with its capabilities (eg. in COVID-19 screening [29], tumour detection [9] and diabetic retinopathy classification [10]). Diagnostic AI has many benefits – freeing up the valuable time of healthcare professionals, quickly analysing large amounts of complex data, and providing efficient diagnoses [32]. It however also comes with drawbacks, including ethical and legal considerations, and reliance on public datasets with imperfect ground truth [20]. The primary drawback of diagnostic AI is the issue of trust – most DL models are ‘black-box’, meaning we cannot see how they work, or which parts of an input are used to generate an output. This has raised issues in the integration of AI into healthcare [2]. The field of Explainable AI (XAI) tackles this by generating explanations that make DL models more easily interpretable. For instance, an image-based Explainable AI (XAI) technique produces a pixel importance heatmap, highlighting the pixels that contributed the most to the classification decision. This allows the user to understand which parts of the image were used by the model, ultimately building trust. Recently, XAI has become a legal requirement for regulatory compliance under acts such

as the EU AI Act ³, which makes *transparent and traceable* decision-making processes mandatory for high-risk systems such as medical diagnostics.

Existing diagnostic XAI techniques are most commonly post-hoc, meaning applied to a pre-trained DL model after classification has taken place. Leading post-hoc XAI techniques perform well in computer vision tasks (eg. object recognition), but tend to be unstable and unreliable when applied to medical datasets [25] [15]. Newer approaches such as LLaVA-Med [16] and CXR-LLaVA [14] instead generate textual explanations for medical images, using a question-answering format where the model is given an image and a diagnosis-related question, and generates a response explaining which parts of the image would contribute to that diagnosis. We explored these models (Section 3.3) and found them unreliable owing to their high sensitivity to the wording of the input question, with a slight re-wording resulting in a completely different response.

We propose an alternative ante-hoc solution based on concept bottleneck models [12], which uses clinical concepts as a middle step to increase the transparency of the classification pipeline. Clinical concepts are extracted from radiology reports associated with the images in our dataset, under direct radiologist guidance. We focus on the binary classification task of lung cancer detection in chest X-rays, using a large public dataset of medical images and associated reports [23]. The classification performance of our model is evaluated against, and outperforms, the state-of-the-art convolutional neural network model, InceptionV3 [28]. We evaluate the interpretability of our approach against post-hoc image XAI techniques LIME [26] and SHAP [19], whose explanations we found to be unstable and clinically irrelevant. We also compare our textual explanations to CXR-LLaVA [14], and find that our explanations more reliably highlight ground truth clinical concepts. Our source code is available on Github⁴.

In summary, we make the following **contributions** in this paper:

- 1) Developed a novel *transparent and clinically interpretable* model for detecting lung cancer in chest X-rays, which utilises information from both free-text medical reports and X-ray images.
- 2) Evaluated and refined our approach under direct guidance of a consultant radiologist to ensure the clinical relevance and usability of our model and its concept-based explanations.

1.1 Related Work

Post-Hoc XAI. Post-hoc image XAI is split into perturbation- and gradient-based techniques. Perturbation-based techniques (eg. LIME [26], RISE [22], SHAP [19]) work by generating random masks of an image to determine which regions have the most effect on a model’s classification decision. Gradient-based techniques (eg. GRADCAM [27], CAM [35], LRP [13]) instead use a forward or backward pass of a DL model to calculate the importance of each input neuron. Many recent studies apply post-hoc image XAI techniques to DL models in the domain of lung pathology classification, uncovering the lack of stability in the explanations produced [24,31]. Explanations from these techniques have been shown to disagree with each other, with the medical ground truth of the dataset and with the opinions of a radiologist [25,15]. Explanations commonly highlight irrelevant regions of medical scans while missing clinical features. GRADCAM

³ <https://artificialintelligenceact.eu/the-act/>

⁴ <https://github.com/AmyRaff/concept-explanations>

[27] has been widely applied to Covid-19 detection models, and was also found to highlight irrelevant regions frequently [1,4,29].

LLM-Based XAI. The recent popularity of ChatGPT [21] and associated open-source large language models (LLMs) has given rise to textual XAI techniques in the form of multimodal models like LLaVA [17], which connect vision encoders and LLMs, usually in a chatbot format. These techniques use Visual Question Answering (VQA) - the process of building models which can answer questions about input images [33,18]. In the medical domain, biomedical chatbots such as LLaVA-Med [16] and CXR-LLaVA [14] have been introduced. We examine the effectiveness of CXR-LLaVA, which is pre-trained on multiple chest X-ray datasets including the one used in this work, for generating clinically relevant lung cancer explanations for Chest X-Rays in Section 3.3.

Concept Bottleneck Models. Our work is based on the concept bottleneck architecture set out by [12], which introduces the idea of splitting a classification pipeline into 2 separate models. The first model takes an image and predicts the presence of a list of pre-determined concepts, and the second takes these concepts and predicts the output label. These concepts act as a convenient middle step to the pipeline, giving the user valuable insight into the decision making process. In this work, we use these concepts as a form of textual XAI, where they are displayed as the justification behind the pipeline’s classification decision.

2 Methodology

As in the original concept bottleneck work [12], our approach splits the traditional Image \rightarrow Label classification pipeline into two separate models (Figure 1). We use a NVIDIA 1060 GTX 6GB GPU for our experiments. The first model in our pipeline is the concept prediction model, which during inference (Figure 1) takes a chest X-ray, and outputs a prediction score for each of the pre-determined list of textual concepts (defined in Section 2.2). Higher scores indicate a higher confidence in the concept’s presence in an image. This model is trained using both chest X-ray images and associated radiology reports, as seen in Figure 2(a). As in the original concept bottleneck work [12,34], we use an InceptionV3-based architecture, trained with a small batch size of 16 and learning rate of 0.0001 due to the size and complexity of our data. The second model is the label prediction model, which during inference (Figure 1) uses the concept prediction scores generated by the previous model to predict the image label (Cancer or Healthy). This model is trained on the radiology reports and pathology labels from our dataset, as seen in Figure 2(b). The original concept bottleneck work uses a Multilayer Perceptron (MLP) model architecture for label prediction. We also experiment with simpler models Support Vector Machines (SVMs) and Decision Trees (DTs) to understand which architecture is most suitable for Chest X-rays.

2.1 Dataset

For this work we use PhysioNet’s large public MIMIC-CXR Dataset of Chest X-rays and associated radiology reports [23,8,3], which includes 227,827 chest X-rays with 14 automatically assigned pathology labels extracted by the CheXpert labelling tool [6]. This dataset contains chest X-rays from multiple viewpoints (PA, AP, lateral) – we focus on the standard PA viewpoint in order to minimise potential confounding variables [11]. As we are focusing on cancer detection,

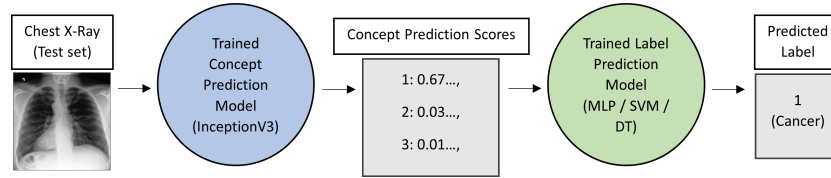


Fig. 1: The inference pipeline for our lung cancer detection approach takes a chest X-ray as input, which is fed into a trained concept prediction model, producing prediction scores for a pre-set list of concepts. These scores are then input to a trained label prediction model, which outputs the binary cancer diagnosis label.

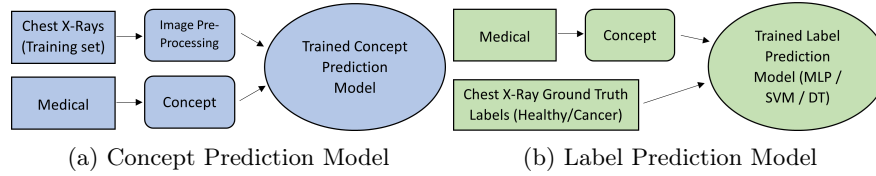


Fig. 2: (a) shows the training pipeline for the concept prediction model taking as input Chest X-Rays and medical reports. (b) shows the label prediction model taking as input medical reports and ground truth pathology labels.

we select only the images labelled as cancerous (Lung Lesion) or healthy (No Finding), under direct radiologist guidance. At this stage our dataset consisted of a significantly higher proportion of healthy scans than cancerous scans – the MIMIC-CXR dataset contains only 1,187 PA chest X-rays labelled Lung Lesion. Although the image data in this dataset could be easily augmented to account for this, generating augmented medical report data while maintaining the link between the report and the image is infeasible. Therefore, we decided to run our experiments with a smaller balanced dataset containing 2,374 scans - all 1,187 cancerous scans and 1,187 randomly selected healthy scans. Images are then scaled to 512x512 pixels, normalized, and cropped to remove black background chunks. We use a test split of 0.1, giving a train/test split of 1923/238.

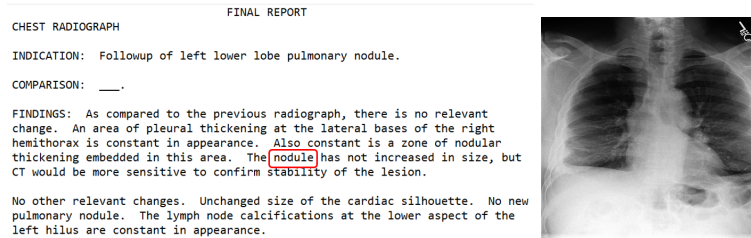


Fig. 3: Example of a cancerous chest X-ray and linked radiology report from the MIMIC-CXR dataset. Clinical concepts extracted ('Nodule') are highlighted by bounding box. Note the negative mention in the final paragraph is not extracted.

CANCER				HEALTHY
Mass	Nodule	Lung cancer	Lymphadenopathy	Normal Unremarkable Lungs clear No evidence
Nodular density	Cavitary lesion	Hilar mass	Pulmonary metastasis	
Nodular densities	Carcinoma	Hilar opacity	Carcinomatosis	
Nodular opacity	Neoplasm	Metastatic disease	Hilar adenopathy	
Nodular opacities	Tumour	Apical opacity	Hilus enlarged	
Nodular opacification	Rounded opacity	Hilar lymphadenopathy	Hilus fullness	

Fig. 4: All 28 clinical concepts as extracted by a trained radiologist.

2.2 Clinical Concept Extraction

Each chest X-ray in our dataset is linked to a free-text radiology report (Figure 3). Report structures vary, so we perform data cleaning under radiologist guidance. Our automated concept extraction focuses only on relevant report sub-sections (FINDINGS and IMPRESSION) [7]. We remove punctuation and unwanted words, generating a list of cleaned sentences for analysis. Then, given a list of clinical concepts in the form of key phrases, we determine which are present in the cleaned report, ignoring negative mentions (Figure 3). We use this information to automatically convert the report into a list of binary values indicating the presence of each concept within the text. To acquire these clinical concepts, a consultant radiologist⁵ analysed a random sample of 100 cancerous and healthy reports, and highlighted key phrases which would have been used in a by-eye diagnosis. After removing duplicates and irrelevant phrases, we were left with 28 clinical concepts – 24 indicating cancer, and 4 indicating a healthy scan (Figure 4). This concept class imbalance is due to the content of our annotated reports. Clinical information indicating pathology presence is significantly more important to medical experts than information indicating a clear scan.

3 Results

We evaluate performance with respect to 1) Concept prediction, 2) Label prediction, and 3) Clinical interpretability compared to existing work.

3.1 Original 28 Concept Model

We initially run our pipeline with the complete set of 28 clinical concepts as extracted by a consultant radiologist (Figure 4). Figure 6 shows the performance of the concept prediction model in terms of accuracy, which we define as the proportion of ground truth concepts captured by the top k highest scoring concepts identified by our model. Considering only the top scoring concept, model accuracy is low at 27.3%. Considering more concepts yields higher accuracy (top 5 = 74.9%, top 10 = 88.1%). We, however, aim to achieve high accuracy with just the top or top few predicted concepts, to maintain the clinical usefulness of our concept-based explanations. An example of a correct explanation using this model is shown in Figure 5(a). Our model correctly classifies this chest X-ray as cancerous, and captures both ground truth concepts (Mass and Lung Cancer) within the top 3 highest scoring concepts. The model, however, also assigns an incorrect concept (Hilar Mass) as the second highest scoring.

⁵ Single expert labelling is commonly used in radiology AI research [5]. Since our clinical concepts are derived from pre-annotated reports and images, bias is mitigated.

Table 1: Label prediction performance for all architectures of our 28-concept and 6-cluster models, compared to the baseline InceptionV3 model.

Model	DT		MLP		SVM		Baseline
	28-Concept	6-Cluster	28-Concept	6-Cluster	28-Concept	6-Cluster	Incep. V3
Precision	0.8235	0.9495	0.5126	0.9411	0.5294	0.9328	0.8487
Recall	0.7000	0.9339	0.8243	0.9333	0.8289	0.9487	0.7214
F1	0.7567	0.9416	0.6321	0.9372	0.6461	0.9407	0.7799

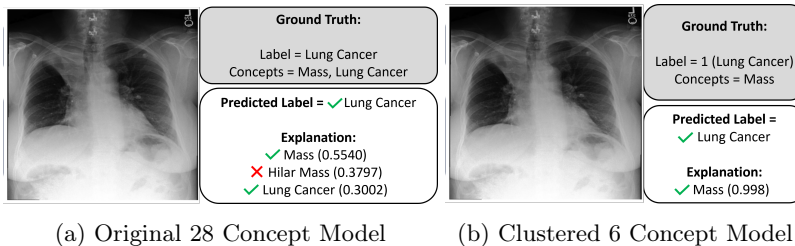


Fig. 5: Explanations generated on a cancerous X-ray by our 28-concept (a) and 6-cluster models (b). Green ticks indicate correct, red cross indicates incorrect.

We consider 3 label prediction model architectures with varying interpretability and complexity - Decision Tree (DT) (most interpretable), SVM, and MLP (most complex). The performances of these models on the 28-concept experiment are shown in Table 1. The DT model performs the best in terms of Precision – we value this metric over Recall, as we are more interested in our model’s ability to identify the positive class (Cancer). We then compare the DT model to our baseline – a 42-layer InceptionV3 model of the same architecture as [30] that instead predicts labels directly from the chest X-ray images. We find our 28-concept DT model has comparable performance to the baseline model (Table 1), despite the poor concept prediction performance.

3.2 Clustered Concept Model

Owing to the poor concept prediction performance of our 28-concept model, we aim to improve our approach via concept clustering to address concept redundancies (eg. Nodular opacity/opacities) and sparsity within our dataset. A consultant radiologist clustered the 28 concepts into 6 categories. Each of these 6 categories represents a meaningful clinical feature commonly used when teaching medical students to manually diagnose chest X-rays - Mass, Nodule, Irregular Hilum, Irregular Lung Parenchyma, Irregular Mediastinum, and Unremarkable. Mass and Nodule refer to detection of areas of opacity within the boundary of the lungs. Unremarkable refers to a Healthy scan with no pathology indicated. The Hilum, Parenchyma and Mediastinum refer to distinct areas within a chest X-ray which may present abnormalities. The concepts within these 6 clusters are shown in Table 2.

The 6-cluster model boasts strong performance in both concept and label prediction. The concept accuracy, as seen in Figure 6, when considering only the top scoring cluster is 97.1%. We believe this improvement is due to the reduction in concept redundancy and sparsity. Table 1 shows the label prediction

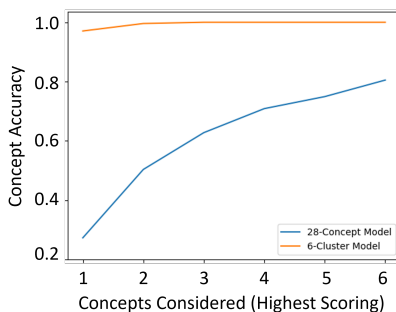


Fig. 6: Concept prediction performances of our 28-concept and 6-cluster models. Only the top 6 concepts of the 28-concept model are shown here for comparison, with the full graph displayed in Figure 9.

performance of our DT, MLP and SVM architectures using the clustered concepts. The performance of all three models are consistently higher than their 28-concept counterparts, and also significantly outperform the baseline InceptionV3 model. The DT model is marginally better than MLP and SVM models with the highest Precision value. It also provides highly accurate textual explanations in the form of the highest scoring concept cluster, as shown in Figure 5(b), where the DT model correctly classifies a chest X-ray as cancerous, and produces the correct explanation using the highest scoring concept cluster ‘Mass’ (matching ground truth). Our approach generates a correct, clinically relevant explanation which tells the user that the X-ray was labelled cancerous due to the presence of a Mass, with over 99% certainty.

3.3 Interpretability

Post-Hoc Comparisons. We compare our concept-based explanations to post-hoc XAI techniques LIME and SHAP, applied to the baseline InceptionV3 model. The image explanations generated by these techniques disagree with each other and the medical ground truth. We show an example of this observation in Figure 7, where both techniques fail to capture the large mass in the X-ray, and highlight irrelevant regions such as areas outside of the lung as incorrectly important to the classification decision. In contrast, our approach correctly identifies the presence of a mass. More examples are shown in Figure 10.

CXR-LLaVA Comparisons. CXR-LLaVA is evaluated in literature through both question answering and automated radiologic report generation. We first explore CXR-LLaVA’s ability to consistently respond to re-wordings of semantically similar questions, finding that diagnosis-implying questions gave diagnosis-assuming responses - examples shown in Figure 8. Unbiased questions (eg. *Do any clinical features of this chest X-ray indicate lung cancer?*) on healthy scans confirmed a lack of lung cancer indications. Diagnosis-implying questions (eg. *Which clinical features of this chest X-ray indicate lung cancer?*) on healthy scans commonly described cancerous regions that did not exist.

To compare our approach to CXR-LLaVA’s ability to generate radiological reports containing correct clinical features, we use a similar approach to [14], where we apply the same NLP concept extraction techniques (Section 2.2) to

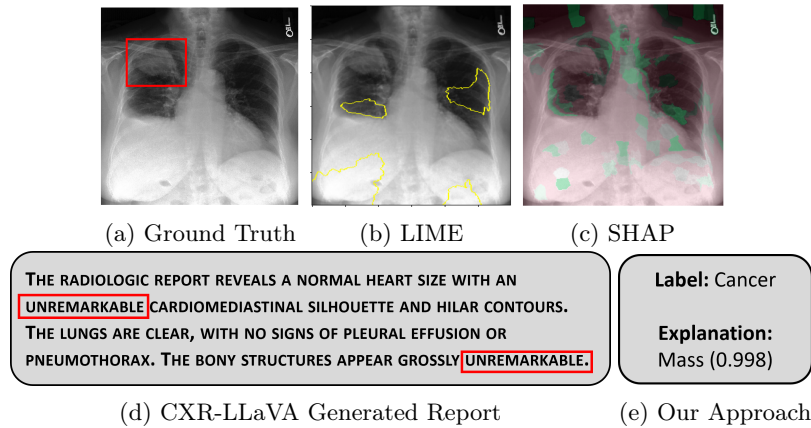


Fig. 7: Example of our explanation approach outperforming LIME, SHAP and CXR-LLaVA. Ground truth (a) is a “**Large right upper zone mass**”. LIME (b) and SHAP (c) fail to capture the mass in the X-ray. Most important image regions are bounded by yellow for LIME, and shown in more vibrant green for SHAP. CXR-LLaVA (d) generates a report which wrongly describes the image as non-cancerous. Our approach (e) correctly identifies the presence of a mass.

both ground truth dataset reports and CXR-LLaVA reports, and compare the proportion of clinical concepts they have in common. We then compare this to the proportion of ground truth concepts captured by our approach’s explanations. We found that CXR-LLaVA’s generated reports were largely false negatives in the context of cancer diagnosis, instead focusing on areas of pneumothorax or cardiomegaly, likely due to imbalances in its training datasets [14]. An example of CXR-LLaVA generating a non-cancerous report for a cancerous scan is shown in Figure 7. On our processed dataset of 2,374 radiological reports (Section 2.1), our concept-based explanations boast a **97.1%** accuracy in capturing the ground truth with the top-1 highest scoring concept cluster. CXR-LLaVA gave an accuracy of **72.6%** on the full dataset, and when considering only cancerous reports this accuracy dropped to **48.3%**. CXR-LLaVA’s reports were competent at explaining diagnosis using mass detection but did not consider other pathology concepts (eg. irregular hilum) which are captured by our approach.

4 Conclusion

In this work we have introduced a novel transparent and explainable AI classification approach for lung cancer detection in chest X-rays. We have shown our approach is more clinically interpretable than LIME, SHAP and textual XAI technique CXR-LLaVA, while significantly outperforming the baseline model in cancer classification performance. We recognise that our experiments are run on a relatively small dataset of 2,374 image-report pairs and we plan to expand this in the future. Additionally, we plan to extend the binary classification task of cancer detection to cover other pathologies seen in chest X-rays.

Disclosure of Interests. The authors have no competing interests to declare that are relevant to the content of this article.

References

1. Brunese, L., Mercaldo, F., Reginelli, A., Santone, A.: Explainable deep learning for pulmonary disease and coronavirus covid-19 detection from x-rays. *Computer Methods and Programs in Biomedicine* **196**, 105608 (2020). <https://doi.org/10.1016/j.cmpb.2020.105608>, <https://www.sciencedirect.com/science/article/pii/S0169260720314413>
2. Farič, N., Hinder, S., Williams, R., Ramaesh, R., Bernabeu, M.O., van Beek, E., Cresswell, K.: Early experiences of integrating an artificial intelligence-based diagnostic decision support system into radiology settings: a qualitative study. (2023)
3. Goldberger, A., Amaral, L., Glass, L., Hausdorff, J., Ivanov, P.C., Mark, R., Stanley, H.E.: Physiobank, physiotoolkit, and physionet: Components of a new research resource for complex physiologic signals. In: *Circulation* [Online] (2000)
4. Haghanifar, A., Majdabadi, M.M., Choi, Y., Deivalakshmi, S., Ko, S.: Covid-cxnet: Detecting covid-19 in frontal chest x-ray images using deep learning (2020)
5. Hosny, A., Parmar, C., Quackenbush, J., Schwartz, L.H., Aerts, H.J.: Artificial intelligence in radiology. *Nature Reviews Cancer* **18**(8), 500–510 (2018)
6. Irvin, J., Rajpurkar, P., Ko, M., Yu, Y., Ciurea-Illcus, S., Chute, C., Marklund, H., Haghighi, B., Ball, R., Shpanskaya, K., Seekins, J., Mong, D.A., Halabi, S.S., Sandberg, J.K., Jones, R., Larson, D.B., Langlotz, C.P., Patel, B.N., Lungren, M.P., Ng, A.Y.: Chexpert: A large chest radiograph dataset with uncertainty labels and expert comparison (2019)
7. Johnson, A., Lungren, M., Peng, Y., Lu, Z., Mark, R., Berkowitz, S., Horng, S.: Mimic-cxr-jpg - chest radiographs with structured labels' (version 2.0.0) (2019)
8. Johnson, A., Pollard, T., Berkowitz, S., et al.: Mimic-cxr, a de-identified publicly available database of chest radiographs with free-text reports. In: *Scientific data*, **6**(1), 317 (2019)
9. Juan, J., Monsó, E., Lozano, C., et al.: Computer-assisted diagnosis for an early identification of lung cancer in chest x rays. (2023)
10. Khalil, H., El-Hag, N., Sedik, A., El-Shafie, W., Mohamed, A.E.N., Khalaf, A.A.M., El-Banby, G.M., Abd El-Samie, F.I., El-Fishawy, A.S.: Classification of diabetic retinopathy types based on convolution neural network (cnn). *Menoufia Journal of Electronic Engineering Research* **28**(ICEEM2019-Special Issue), 126–153 (2019)
11. Kim, D., Chung, J., Choi, J., et al.: Accurate auto-labeling of chest x-ray images based on quantitative similarity to an explainable ai model. (2022)
12. Koh, P.W., Nguyen, T., Tang, Y.S., Mussmann, S., Pierson, E., Kim, B., Liang, P.: Concept bottleneck models (2020)
13. Lapuschkin, S., Binder, A., Montavon, G., Klauschen, F., Müller, K.R., Samek, W.: On pixel-wise explanations for non-linear classifier decisions by layer-wise relevance propagation. *PLoS ONE* **10**, e0130140 (07 2015). <https://doi.org/10.1371/journal.pone.0130140>
14. Lee, S., Youn, J., Kim, H., Kim, M., Yoon, S.H.: Cxr-llava: a multimodal large language model for interpreting chest x-ray images (2024)
15. Legastelois, B., Rafferty, A., Brennan, P., Chockler, H., Rajan, A., Belle, V.: Challenges in explaining brain tumor detection. In: *Proceedings of the First International Symposium on Trustworthy Autonomous Systems. TAS '23*, Association for Computing Machinery, New York, NY, USA (2023). <https://doi.org/10.1145/3597512.3600208>
16. Li, C., Wong, C., Zhang, S., Usuyama, N., Liu, H., Yang, J., Naumann, T., Poon, H., Gao, J.: Llava-med: Training a large language-and-vision assistant for biomedicine in one day (2023)
17. Liu, H., Li, C., Wu, Q., Lee, Y.J.: Visual instruction tuning (2023)
18. Liu, Y., Wang, Z., Xu, D., Zhou, L.: Q2atransformer: Improving medical vqa via an answer querying decoder (2023)

19. Lundberg, S., Lee, S.: A unified approach to interpreting model predictions. In: Proceedings of the 31st international conference on neural information processing systems. pp. 4768 – 4777 (2017)
20. Oakden-Rayner, L.: Exploring the chestxray14 dataset: problems. LaurenOakdenRayner (2017), <https://laurenOakdenrayner.com/2017/12/18/the-chestxray14-dataset-problems/>
21. OpenAI: Chatgpt (2024)
22. Petsiuk, V., Das, A., Saenko, K.: RISE: Randomized input sampling for explanation of black-box models. In: arXiv, 1806.07421 (2018)
23. PhysioNet: Mimic-cxr dataset. <https://physionet.org/content/mimic-cxr/2.0.0/> (2019), accessed: 28.02.2024
24. Pitroda, V., Fouda, M.M., Fadlullah, Z.M.: An explainable ai model for interpretable lung disease classification. In: 2021 IEEE International Conference on Internet of Things and Intelligence Systems (IoT&IS). pp. 98–103 (2021). <https://doi.org/10.1109/IoT&IS53735.2021.9628573>
25. Rafferty, A., Nenutil, R., Rajan, A.: Explainable artificial intelligence for breast tumour classification: Helpful or harmful. In: Interpretability of Machine Intelligence in Medical Image Computing. pp. 104–123. Springer Nature Switzerland, Cham (2022)
26. Ribeiro, M., Singh, S., Guestrin, C.: "Why should I trust you?": Explaining the predictions of any classifier. In: arXiv, 1602.04938v3 (2016)
27. Selvaraju, R.R., Cogswell, M., Das, A., Vedantam, R., Parikh, D., Batra, D.: Grad-CAM: Visual explanations from deep networks via gradient-based localization. International Journal of Computer Vision **128**(2), 336–359 (oct 2019). <https://doi.org/10.1007/s11263-019-01228-7>
28. Shadin, N.S., Sanjana, S., Lisa, N.J.: Covid-19 diagnosis from chest x-ray images using convolutional neural network (cnn) and inceptionv3. In: 2021 International Conference on Information Technology (ICIT). pp. 799–804. IEEE (2021)
29. Singh, R., Pandey, R., Babu, R.: Covidscreen: explainable deep learning framework for differential diagnosis of covid-19 using chest x-rays. (2021)
30. Szegedy, C., Vanhoucke, V., Ioffe, S., Shlens, J., Wojna, Z.: Rethinking the inception architecture for computer vision (2015)
31. Vermeire, T., Brughmans, D., Goethals, S., et al.: Explainable image classification with evidence counterfactual. In: Pattern Anal Applic 25, 315–335 (2022)
32. Wang, J.: The power of ai-assisted diagnosis. EAI Endorsed Transactions on e-Learning **8**(4) (9 2023). <https://doi.org/10.4108/eetel.3772>
33. Y, B., MMA, R., L, B., M., Z.: Vision-language model for visual question answering in medical imagery. In: Bioengineering (Basel). 2023 Mar 20;10(3):380. (2023)
34. yewsiang: Conceptbottleneck. <https://github.com/yewsiang/ConceptBottleneck> (2022), accessed: 28.02.2024
35. Zhou, B., Khosla, A., Lapedriza, A., Oliva, A., Torralba, A.: Learning deep features for discriminative localization. In: arXiv, 1512.04150 (2016)

Table 2: Concept clustering as performed by an NHS radiologist. The original 28 concepts are clustered into 6 categories.

Cluster	Concepts
Mass	Mass, Cavitory lesion, Carcinoma, Neoplasm, Tumor, Rounded opacity, Lung cancer, Apical opacity
Nodule	Nodular density, Nodular densities, Nodular opacity, Nodular opacities, Nodular opacification, Nodule
Irregular Hilum	Hilar mass, Hilar opacity, Hilar adenopathy, Hilus enlarged, Hilus fullness, Hilar lymphadenopathy
Irregular Lung Parenchyma	Pulmonary metastasis, Carcinomatosis, Metastatic disease
Irregular Mediastinum	Lymphadenopathy
Unremarkable	Normal, Unremarkable, Lungs clear, No evidence

Does this chest X-ray contain any indications of lung cancer? No, there is no evidence of lung cancer in this chest X-ray.	Does this chest X-ray contain any indications of lung cancer? No, there are no indications of lung cancer in this chest X-ray.
Do any clinical features of this chest X-ray indicate lung cancer? No, there are no clinical features of this chest X-ray that suggest the presence of lung cancer.	Do any clinical features of this chest X-ray indicate lung cancer? No, there are no clinical features of this chest X-ray that suggest the presence of lung cancer.
Which clinical features of this chest X-ray indicate lung cancer? The presence of a right apical mass and the absence of consolidation suggest lung cancer.	Which clinical features of this chest X-ray indicate lung cancer? The presence of a right pectoral Port-A-Cath and left axillary clips are indicative of lung cancer.

Fig. 8: Examples of CXR-LLaVA having inconsistent answers to re-worded questions of the same meaning. If a diagnosis is implied in the question, the model generates a response assuming the diagnosis. These questions were asked on healthy scans with no indication of lung cancer.

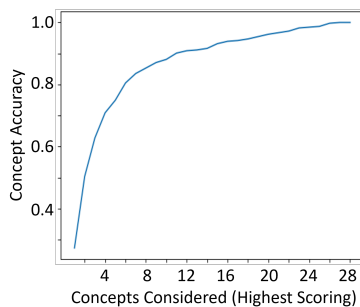


Fig. 9: Concept prediction performance of 28-concept model for all 28 concepts.

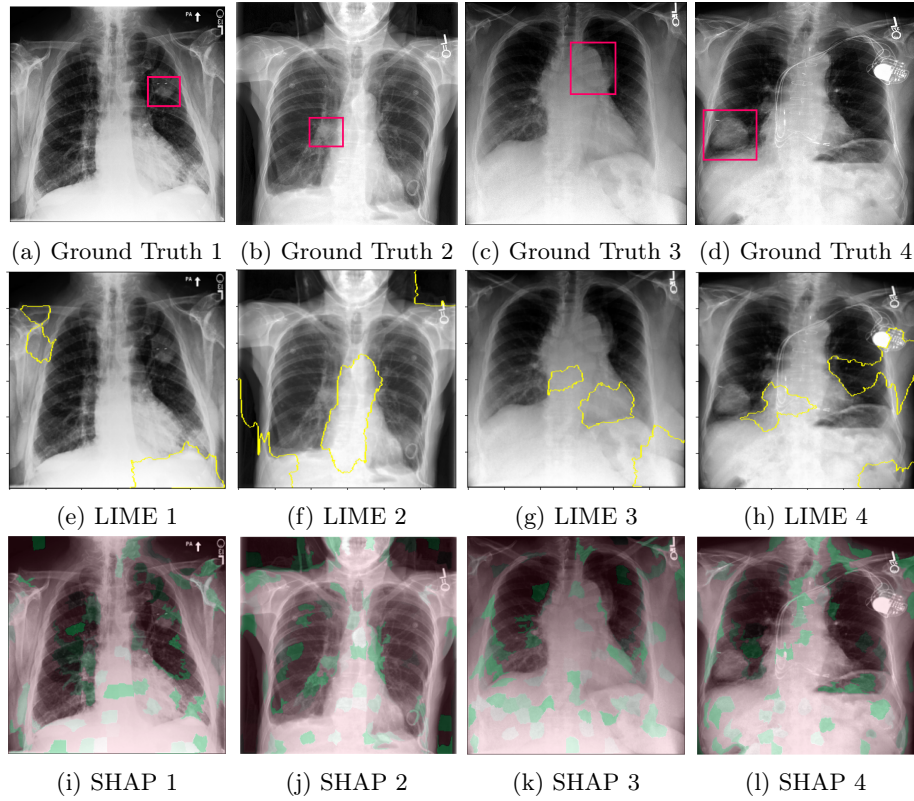


Fig. 10: Examples of LIME and SHAP explanations failing to capture the medical ground truth of a cancerous chest X-ray, while also generating conflicting explanations. Ground truth (a,b,c,d) is shown as red squares. Most important regions are bounded by yellow for LIME (e,f,g,h) and shown as more vibrant green for SHAP (i,j,k,l).